nature materials

SUPPLEMENTARY INFORMATION

https://doi.org/10.1038/s41563-019-0370-z

In the format provided by the authors and unedited.

Long-range chiral exchange interaction in synthetic antiferromagnets

Dong-Soo Han[1,2,3,8], Kyujoon Lee[1,8], Jan-Philipp Hanke[1,4], Yuriy Mokrousov[1,4], Kyoung-Whan Kim[2], Woosuk Yoo[5], Youri L. W. van Hees[3], Tae-Wan Kim[6], Reinoud Lavrijsen[3], Chun-Yeol You[7], Henk J. M. Swagten[3], Myung-Hwa Jung[5]* and Mathias Kläui[1]*

[1]Institute of Physics, Johannes Gutenberg-Universität Mainz, Mainz, Germany. [2]Center for Spintronics, Korea Institute for Science and Technology, Seoul, Republic of Korea. [3]Department of Applied Physics, Institute for Photonic Integration, Eindhoven University of Technology, Eindhoven, The Netherlands. [4]Peter Grünberg Institut and Institute for Advanced Simulation, Forschungszentrum Jülich and JARA, Jülich, Germany. [5]Department of Physics, Sogang University, Seoul, Republic of Korea. [6]Department of Advanced Materials Engineering, Sejong University, Seoul, Republic of Korea. [7]Department of Emerging Materials Science, DGIST, Daegu, Republic of Korea. [8]These authors contributed equally: Dong-Soo Han, Kyujoon Lee.
*e-mail: mhjung@sogang.ac.kr; klaeui@uni-mainz.de

Supplementary Information

Long-range chiral exchange interaction in synthetic antiferromagnets

Dong-Soo Han[1,2,3†], Kyujoon Lee[1†], Jan-Philipp Hanke[1,4], Yuriy Mokrousov[1,4], Kyoung-Whan Kim[2], Woosuk Yoo[5], Youri L. W. van Hees[3], Tae-Wan Kim[6], Reinoud Lavijsen[3], Chun-Yeol You[7], Henk J. M. Swagten[3], Myung-Hwa Jung[5*], and Mathias Kläui[1*]

1. Institute of Physics, Johannes Gutenberg-Universität Mainz, 55099, Mainz, Germany

2. Center for Spintronics, Korea Institute for Science and Technology, Seoul, Republic of Korea.

3. Department of Applied Physics, Institute for Photonic Integration,Eindhoven University of Technology, P.O. Box 513, 5600 MB Eindhoven, The Netherlands

4. Peter Grünberg Institut and Institute for Advanced Simulation, Forschungszentrum Jülich and JARA, 52425 Jülich, Germany

5. Department of Physics, Sogang University, Seoul, Republic of Korea.

6. Department of Advanced Materials Engineering, Sejong University, Seoul 04107, Republic of Korea

7. Department of Emerging Materials Science, DGIST, Daegu 42988, Republic of Korea

S1. Asymmetric magnetic hysteresis loops by chiral magnetization configurations

To provide a more comprehensive understanding of the asymmetric and unidirectional magnetization reversal by the chiral magnetization configurations, here we discuss magnetic hysteresis loops under an applied in-plane field H_{IN}. Figure S1a shows the magnetic hysteresis loops in a synthetic antiferromagnet (SAF) with antiparallel coupling. Arrows and the enumeration of 1-4 indicate the four representative magnetization states of parallel and the antiparallel magnetization alignments. A key feature of the magnetic hysteresis loops is that the switching fields for each state show different behaviors under H_{IN}. For the switching from antiparallel to parallel alignment corresponding to the switching from 1 to 2 and 3 to 4 state, the switching fields for both up-to-down (U-D) and down-to-up (D-U) switching are moved into the direction on which $|H_{SW}|$ increase. However, the relative change in the switching field exhibits different behaviors according to the sign of H_{IN} and the switching polarity: for the switching from 1 to 2 state, the change in H_{SW} is smaller than that for the switching from 3 to 4 state at $\mu_0 H_{IN}$ = 100 mT, and vice versa at $\mu_0 H_{IN}$ = -100 mT. Whereas, for the switching from antiparallel to parallel alignment, the change of H_{SW} is negligible for the switching from 2 to 3 but $|H_{SW}|$ decreases for the switching from 4 to 1 at $\mu_0 H_{IN}$ = 100 mT, and vice versa at $\mu_0 H_{IN}$ = -100 mT. This H_{IN}- and magnetization-state-dependent switching behavior is in disagreement with the general feature that the H_{IN} assists the magnetization reversal irrespectively of the magnetization states and the sign of H_{IN} (see Fig. S1b), implying that there exists a hidden interaction breaking the field-reversal symmetry. Note that the H_{IN}- and magnetization-state-dependent switching behavior is a unique signature of the chiral magnetization configurations. For SAF with antiparallel coupling, when H_{IN} assists the magnetization reversal, the magnitude of H_{SW} is generally increased as H_{IN} increases for the switching from parallel to antiparallel alignment, whereas it decreases for the switching from antiparallel to parallel alignment. This is because the antiparallel magnetization configuration

is a favored state, so the switching from the parallel to antiparallel (antiparallel to parallel) alignment requires more (less) energy for the magnetization reversal when it is assisted by H_{IN}. This is in agreement with the hysteresis loops in Fig. S1b, as calculated neglecting the *antisymmetric interlayer* exchange interaction (IEI). In this context, the measured switching behavior can be understood as follows: for both switching from 1 to 2 and 2 to 3, the magnetization reversal is more assisted by positive H_{IN} than by negative H_{IN}, but vice versa for the switching from 3 to 4 and 4 to 1. This is in perfect agreement with the chiral magnetization configurations and the effect of H_{IN} on their switching, as schematically drawn in Fig. S1c.

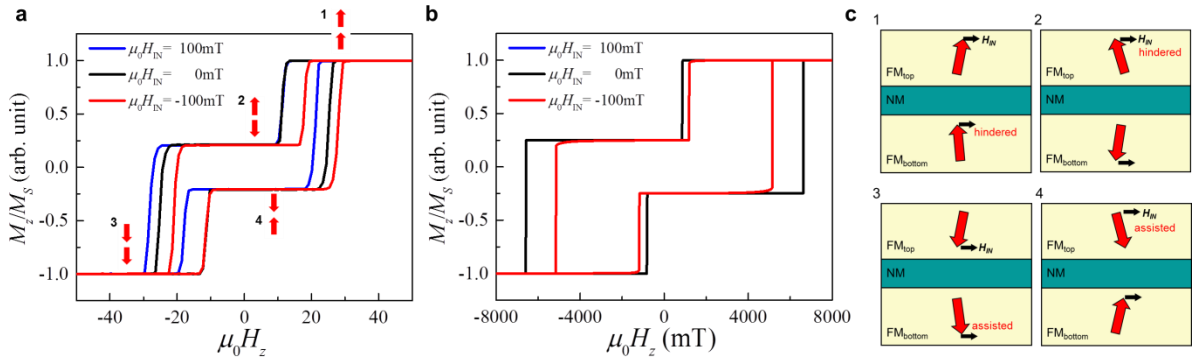

Figure S1. Asymmetric hysteresis loops by H_{IN}. a, Hysteresis loops measured for synthetic antiferromagnet (SAF) with antiparallel coupling under the in-plane field $\mu_0 H_{IN}$ = 0 and ± 100 mT applied along asymmetric (**AS**) axis, as defined in Fig. 2. The red arrows represent the magnetization direction of the two different ferromagnetic layers of the SAF. The four representative alignments are numbered. **b**, Numerically calculated hysteresis loops of SAF with antiparallel *symmetric* IEI but without *antisymmetric* IEI. The red and blue lines are superimposed. **c**. Schematic illustration of chiral magnetization configuration of four different magnetic states and the effect of H_{IN} on the magnetization reversal. The black arrows show the in-plane field acting on the magnetization. All magnetization configurations have the same chirality of the right-handedness.

S2. Other possible contributions to asymmetric hysteresis loops

2.1 Biquadratic *interlayer* exchange interaction.

Besides the *symmetric* IEI, an additional non-Heisenberg IEI, namely the biquadratic IEI, may manifest in SAFs as attributed to a lateral inhomogeneity that gives rise to local fluctuations of the *symmetric* IEI.[1,2] This biquadratic IEI is generally expressed as $-J_2(\mathbf{m}_1 \cdot \mathbf{m}_2)^2$, where J_2 denotes the coupling constant, $\mathbf{m}_1$ and $\mathbf{m}_2$ are the magnetization vectors of the two coupled layers.[1] Hence, the effect can also lead to the non-collinear spin structures as suspected to be in our samples. However, this cannot account for the chiral and unidirectional features demonstrated as described in the main text, as it has an isotropic nature as the *symmetric* IEI. Figure S2 shows the numerically calculated the azimuthal-angular dependence of switching field that is obtained by taking into account the biquadratic IEI and *symmetric* IEI under the application of $|\mu_0 H_{IN}|$ = 50 mT. The results clearly demonstrate that the switching fields for U-D and D-U switching of both the bottom and top layers become isotropic, as expected. Therefore, we conclude that the biquadratic IEI can be ruled out as the origin of the phenomena we observed.

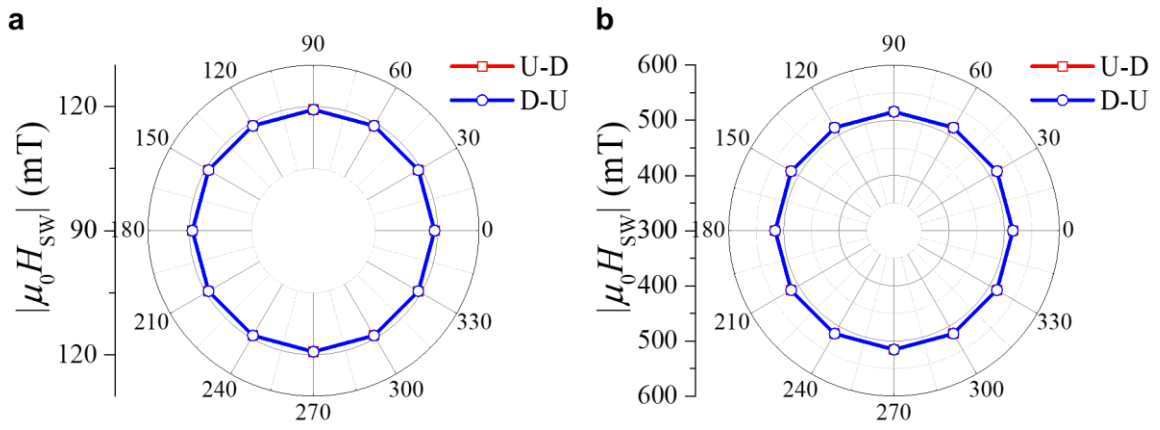

Figure S2 Numerically calculated azimuthal-angular dependence of switching fields from biquadratic interlayer exchange interaction. **a**, Azimuthal-angular dependence of switching fields H_{SW} for the bottom layer of synthetic antiferromagnet (SAF) with antiparallel coupling, as

obtained from numerical calculation taking into account Zeeman energy, anisotropy energy, *symmetric* interlayer exchange interaction (IEI), and biquadratic IEI. **b**, Azimuthal-angular dependence of switching fields for the top layer of SAF with antiparallel coupling. The red and blue lines represent for up-to-down (U-D) and down-to-up (D-U) switching polarities, respectively. The blue and red lines are superimposed for both graphs.

2.2 *Intralayer* Dzyaloshinskii-Moriya interaction combined with the *symmetric interlayer* exchange interaction.

As described and demonstrated by studying a laterally symmetric reference sample and previous studies about the *intralayer* Dzyaloshinskii-Moriya interaction (DMI),[3–5] although the *intralayer* DMI can break the field-reversal symmetry of the domain wall dynamics,[4] this cannot solely lead to the asymmetric magnetic hysteresis loops of which coercive fields are predominantly determined by the nucleation field of reversed domains. An asymmetric magnetic hysteresis loop can only appear when it is assisted by additional symmetry breaking effects, such as laterally asymmetric microstructures[5] and spin currents with a fixed spin polarization which all give rise to additional out-of-plane fields,[3,6] but this is not our case (see Fig. S3a).

In this section, we further discuss whether the *intralayer* DMI can lead to the appearance of the unidirectional and chiral features, particularly, in combination with the *symmetric* IEI, from simple symmetry considerations as well as micromagnetic simulations.

Let us first discuss the effect of the *intralayer* DMI and the *symmetric* IEI from a simple symmetry argument. In a lack of the inversion symmetry breaking (ISB) such as the *antisymmetric* IEI in the plane of thin films, the magnetic multilayers with the *intralayer* DMI at each interface, the *symmetric* IEI, and magnetic anisotropy lies in a $C_{n\mathrm{v}}$ symmetry class where n >1, as individual magnetic energies have an in-plane symmetry higher than $C_{2\mathrm{v}}$. Note that although the *intralayer* DMI arises due to the ISB at interfaces (out-of-plane) it still has a

high symmetry in the plane of magnetic thin films. This in-plane symmetry of the magnetic system leads to the identical magnetic behaviors for the following magnetic configurations (Fig. S3 *a*-*c*) given by two different rotation operations. First, for the case where the magnetic multilayers and magnetic fields applied to the system are all rotated by 180˚ with respect to the axis perpendicular to the thin films (*z*-axis), the two different configurations (configuration **a** and **b**) in Fig. S3 are equivalent by symmetry, thereby, it is apparent that they should give the equivalent switching fields. By contrast, for the case where the magnetic multilayers are solely rotated by 180° around *z*-axis, the magnetic behaviors of the configurations (**b**) and (**c**) can be differentiated by the in-plane field depending on the symmetry of the individual magnetic interactions in the magnetic system. However, as aforementioned above, the *intralayer* DMI, the *symmetric* IEI, and magnetic anisotropy energy with the symmetry higher than C_{2v} should be all equivalent to the inversion of the in-plane magnetic field, therefore, two configurations of (**b**) and (**c**) are energetically equivalent, implying that hysteresis curves under application of B_x and $-B_x$ should be identical for a certain magnetic configuration (see configurations **a** and **c**). This is clearly in contrast to our experimental observation that magnetic configurations (**a**) and (**c**) show different switching fields. This general symmetry argument implies that our experimental results cannot be accounted for by the existing mechanisms such as *intralayer* DMI and the *symmetric* component of IEI as well as the magnetic anisotropy with the high order contributions.

The symmetry argument can be also given by simple mathematical formulations. We denote the magnetic energy functional of the system by $E(\mathbf{m}_1, \mathbf{m}_2)$ where $\mathbf{m}_1$ and $\mathbf{m}_2$ are magnetization unit vectors of top and bottom layers, respectively. In the absence of the *antisymmetric* IEI, the C_{nv} symmetry has an invariance under rotation around z by $2\pi/n$. Denoting the corresponding rotation by $\mathcal{R}$, this is equivalent to

$$E(\mathbf{m_1}, \mathbf{m_2}) = E(\mathcal{R}\mathbf{m}_1, \mathcal{R}\mathbf{m}_2).$$

Now, we consider an external magnetic field $\mathbf{B}_{\text{ext}} = B_x\hat{x} + B_z\hat{z}$ where $\hat{x}$ and $\hat{z}$ are the unit vectors in the x and z direction respectively. B_x and B_z are the x and z components of the external field. Then, it is straightforward to show that

$$E(\mathbf{m_1}, \mathbf{m_2}) - (\mathbf{m_1} + \mathbf{m_2}) \cdot (B_x\hat{x} + B_z\hat{z})$$
$$= E(\mathcal{R}\mathbf{m}_1, \mathcal{R}\mathbf{m}_2) - (\mathcal{R}\mathbf{m}_1 + \mathcal{R}\mathbf{m_2}) \cdot (B_x\mathcal{R}\hat{x} + B_z\hat{z}).$$

Note that the hysteresis loop measures m_z component, which is invariant under $\mathcal{R}$, the hysteresis loop obtained from $(\mathbf{m_1}, \mathbf{m_2})$ and that obtained from $(\mathcal{R}\mathbf{m_1}, \mathcal{R}\mathbf{m_2})$ should be identical. Therefore, we conclude that the hysteresis loops for $\mathbf{B}_{\text{ext}} = B_x\hat{x} + B_z\hat{z}$ and $\mathbf{B}_{\text{ext}} = B_x\mathcal{R}\hat{x} + B_z\hat{z}$ are identical. Note that the aforementioned and illustrated in Fig. S3 cases correspond to a special case of $\mathcal{R}\hat{x} = -\hat{x}$, but this general symmetry argument can apply to any rotation operation of $\mathcal{R}$.

There are two side remarks. First, in real situations, there could be a number of local defects which may locally break the $C_{n\underline{v}}$ symmetry. However, such an effect can be excluded for a large sample - that is our case, as it will be averaged out. Second, this symmetry argument may require more careful consideration if the energy functional $E(\mathbf{m_1}, \mathbf{m_2})$ has more than one minimum, possibly resulting in random behaviors of switching fields. But, this also can be ruled out by the systematic and repetitive measurements performed with various magnetic fields.

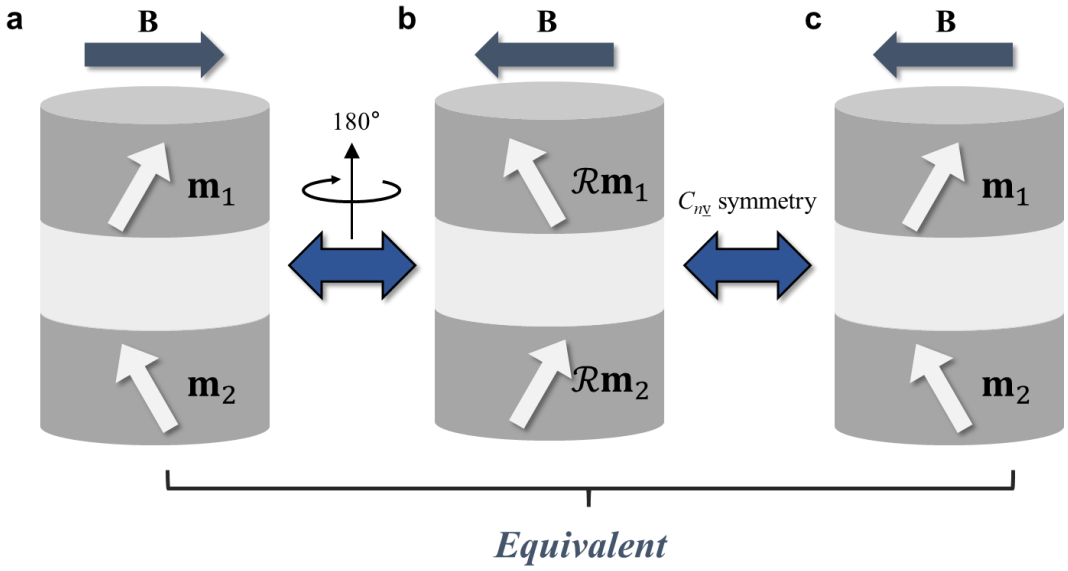

Figure S3. **Three equivalent configurations in magnetic systems with $C_{n\underline{v}}$ symmetry.** **a,** The magnetic multilayer system before considering a rotation. The white arrows represent the magnetization directions of m_1 and m_2 of the different ferromagnets. The dark blue arrow represents the direction of the in-plane bias field. **b,** The system after rotation of magnetic multilayers and magnetic fields by 180° around *z*. (**a**) and (**b**) are equivalent by symmetry. **c,** The system after rotation of magnetic multilayers by 180° around *z*. For the magnetic systems with $C_{n\underline{v}}$ symmetry for all consisting interactions, the configuration (**b**) and (**c**) are equivalent under the inversion of the magnetic fields. Therefore, configuration (**a**), (**b**), and (**c**) should be all equivalent for $C_{n\underline{v}}$ symmetry systems.

In addition to the symmetry argument, we also explored this effect by micromagnetic simulations taking into account the *symmetric* IEI, the *intralayer* DMI, and the perpendicular magnetic anisotropy. We employed the OOMMF code incorporating the Landau-Lifshitz-Gilbert (LLG) equation of motion of magnetization. In our calculations, we used the following material parameters: saturation magnetization M_s = 1.1×10^6 A/m, exchange stiffness A = 10×10^{-12} J/m, uniaxial anisotropy K_U = 9.83×10^5 and 10.5×10^5 J/m^3 for the bottom and top layers, respectively. The exchange coefficient for the *symmetric* IEI we used is J_{sym} = -10.5×10^{-5} mJ/m^2. For the *intralayer* DMI, we used $|D|$ = 0.5 mJ/m^2 for both top and bottom ferromagnetic layers. Two different cases of which the top and bottom layers have the

same and opposite sign of the effective DMI are considered. Figure S4 shows the calculated hysteresis loops at $\mu_0 H_{IN}$ = 0 and ±200 mT. When H_{IN} is applied, H_{SW} change by H_{IN}. However, we found that H_{IN} affects the hysteresis loops identically for all switching cases irrespectively of the switching polarity and the sign of H_{IN}, leading to the symmetric magnetic hysteresis loops around H_z. This reveals that the *intralayer* DMI combined with the *symmetric* IEI cannot produce chiral and asymmetric magnetization reversal by H_{IN}, and H_{IN} only assist the magnetization switching.

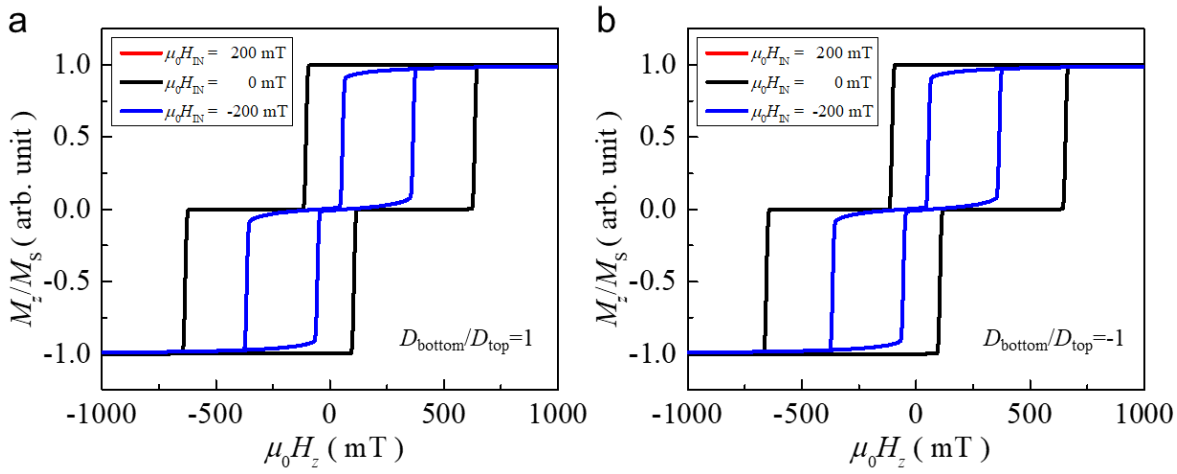

Figure S4. The effect of *intralayer* Dzyaloshinskii-Moriya interaction and *symmetric* interlayer exchange interaction on magnetic hysteresis loops. a, Magnetic hysteresis loops calculated by micromagnetic simulations with an in-plane bias field $\mu_0 H_{IN}$ = 0 and ± 200 mT for the case where the *intralayer* Dzyaloshinskii-Moriya interaction of the top (D_{top}) and bottom layers (D_{bottom}) are the same. The red and blue lines represent the case when $\mu_0 H_{IN}$ = 200 and -200 mT respectively. **b**, Magnetic hysteresis loops for D_{bottom}/D_{top} = -1. The blue and red lines are superimposed for both graphs.

2.3 High-order magneto-crystalline anisotropy energy

In the presence of the ISB, the magneto-crystalline anisotropy energy can also contain an *antisymmetric* term that is odd upon the magnetization reversal[7] , accordingly, leading to asymmetric hysteresis loops as well. The magneto-crystalline anisotropy energy up to fourth

order, then, can be expressed as: $E(\theta,\varphi) = -K_1\cos^2\theta - K_2\cos^4\theta - K_3\cos\theta\sin^3\theta\cos 3\varphi$, where the θ and φ represent the polar and azimuthal angle of the magnetization respectively. K_1, K_2, and K_3 denote the constant of the first, second, and fourth order surface anisotropy. In general, this effect is tiny, so it is neglected in most cases. However, this can presumably compete with the asymmetric IEI, as both are small in amplitude. Here, we explore the effect of the asymmetric anisotropy energy on the magnetization reversal by numerical calculations of the macro-spin model.

In our calculations, we took into account Zeeman energy, anisotropy energy, and *symmetric* exchange interaction. For the anisotropy energy, in order to see the effect better, we used K_3 corresponding to $K_3/K_1 = 0.03$, which is two orders of magnitude larger than realistic values. Note that, for simplicity, here we neglect the second order anisotropy K_2 that may quantitatively affect the switching fields but would not significantly alter the qualitative features. Furthermore, in our calculations, we assumed that the asymmetric anisotropy term exists only in the top layer. This is justified, as the reference sample of Pt/Co/Pt/Ru nominally identical to the bottom half of SAFs with parallel and antiparallel couplings does not show any unidirectional feature. Figure S5 show the azimuthal-angular dependence of the calculated switching fields in SAFs with antiparallel coupling. Although the unidirectional behavior is seen for the top layer attributed to the asymmetric anisotropy term, however, the isotropic behavior is seen in the bottom layers. This evidences that although asymmetric anisotropy from the high-order magneto-crystalline anisotropy can give rise to the unidirectional anisotropy in the magnetization switching field, it exists independently in each magnetic layer, therefore, the chiral behavior between the top and bottom Co layers cannot be accounted by this effect.

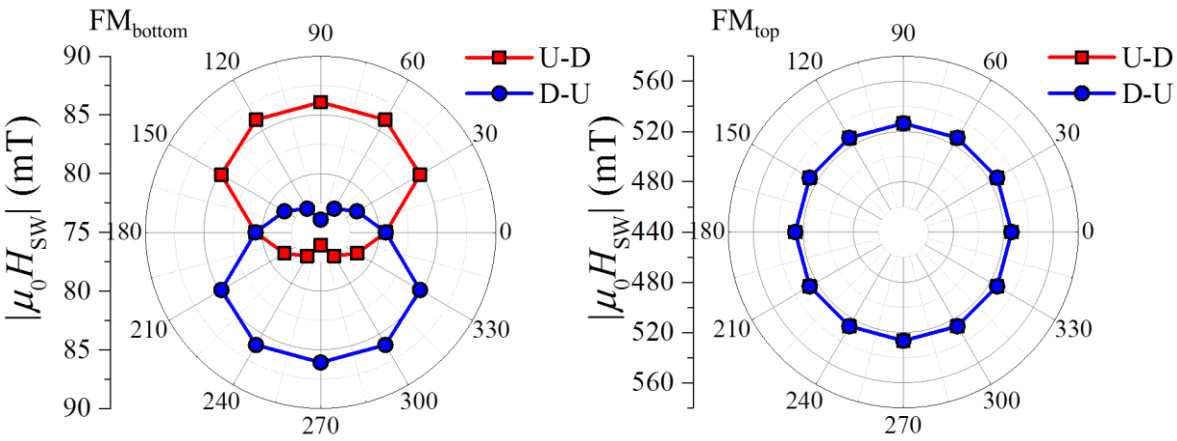

Figure S5. Asymmetric switching behaviors by high-order asymmetric magneto-crystalline anisotropy. Azimuthal-angular dependence of switching field H_{SW} for synthetic antiferromagnet with antiparallel coupling in the presence of the high-order asymmetric magneto-crystalline anisotropy. The two rows show the results for the top and bottom ferromagnetic layer. The red and blue symbols represent the up-to-down (U-D) and down-to-up (D-U) switching of the magnetic layers. Only a unidirectional feature is observed for the top magnetic layer. The red and blue lines are superimposed for the right panel.

S3. Azimuthal-angular dependence of switching field in SAFs with parallel and antiparallel coupling

The azimuthal-angular dependence of switching fields from numerical calculations is discussed in this section. In our calculations, the same material parameters and interactions as discussed in the main text and methods are used and an arbitrarily defined *antisymmetric* IEI vector, $\hat{D}=[010]$, which is along the 90°-270° line in Fig. S6, is considered. Figure S6 shows the calculated azimuthal-angular dependence of switching fields. Interestingly, qualitatively similar behaviors to the experimental observations – chiral and unidirectional behaviors - are seen, although the direction of the asymmetric (**AS**) and symmetric (**S**) axes (see Fig 3) which are dependent on the selection of the *D* vector is found to be different to those from experimental data. We note that **AS** and **S** axes are always perpendicular and parallel, respectively, to the *D* vector. This is due to the fact that the chiral tilting between the magnetizations appears perpendicularly to the *D* vector. Hence, only the in-plane field component along the tilting axis can break the field-reversal symmetry, leading to the difference in Zeeman energy.

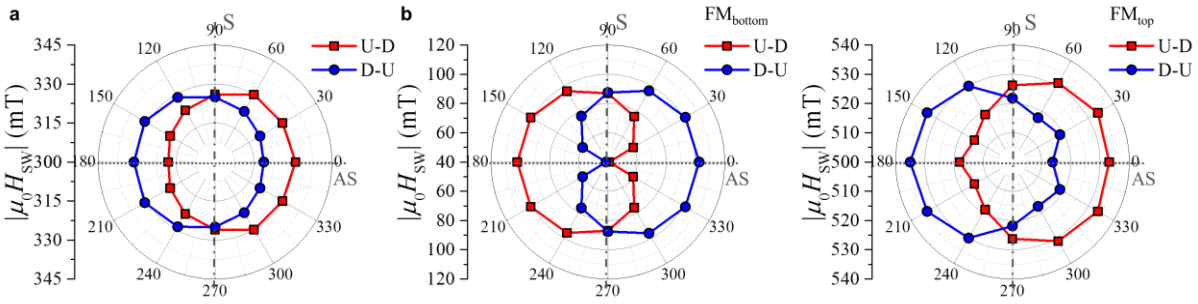

Figure S6 Numerically calculated switching fields in synthetic antiferromagnets with *antisymmetric* interlayer exchange interaction. a, Azimuthal-angular dependence of switching field in synthetic antiferromagnets (SAFs) with parallel coupling, as calculated in consideration of the *antisymmetric* interlayer exchange interaction. The red and blue symbols represent the up-to-down (U-D) and down-to-up (D-U) switching of the ferromagnetic layers. **AS** and **S** represent asymmetric and symmetric axes, respectively. **b**, Azimuthal-angular dependence of switching field in SAFs with antiparallel coupling. The left and right panel of (**b**) represent switching fields for the bottom and top

magnetic layers, respectively. All the results show a unidirectional characteristic in the azimuthal-angular dependence of H_{SW}.

S4. Details about the ab initio calculations

In order to evaluate the chiral IEI, we perform ab-initio calculations of the energy dispersion of coned spin spirals[8] that propagate perpendicular to the film plane. The spin rotation axis is oriented perpendicular to the mirror plane in the C_{1v} systems such that the collinear magnetic moments in layer i follow the equation

$$\mathbf{S}_i = \left(\cos\beta,\ \sin\beta\sin qR_i, -\sin\beta\cos qR_i\right)$$

Here, the wave vector **q** = (0, 0, *q*) of the spin spiral is characterized by the scalar *q*, the small cone angle ß typically amounts to 10°, and R_i denotes the *z* position of the ith magnetic layer. Introducing the relative canting angle $\alpha = q(R_i - R_j)$ between the two adjacent ferromagnetic layers *i* and *j*, we can determine effective coupling constants based on the energy dispersion $E(\alpha)$ of the spin-spiral state:

$$D_{\text{inter}} = -\frac{E(\alpha)-E(0)}{\sin^2\beta\sin\alpha},$$
$$J_{\text{inter}} = -\frac{E(\alpha)-E(0)}{\sin^2\beta\left(\cos\alpha-1\right)}.$$

While using a small cone angle β ensures that the magnetic force theorem can be applied, the corresponding energy scale of spin-orbit induced changes in the dispersion of spin spirals is on the order of tens of μeV (see Fig. S7), which necessitates a dense sampling of the momentum Brillouin zone.

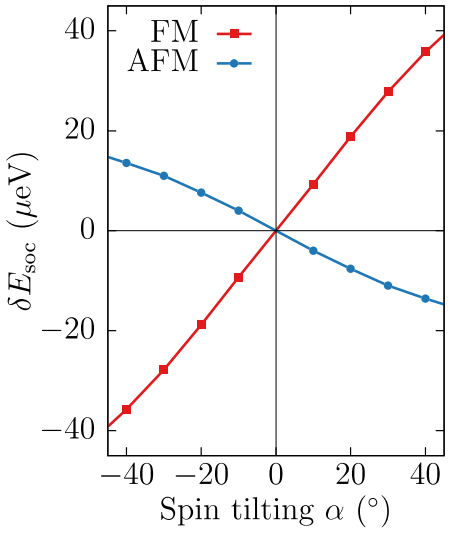

Figure S7. First-principles calculation of chiral interlayer exchange interation. The chiral interlayer exchange interaction manifests in a spin-orbit induced contribution δE_{soc} to the total energy, which is antisymmetric with respect to the relative canting angle α between the collinear magnetic layers. The data are shown for an overall ferromagnetic or antiferromagnetic coupling of the magnets with the top Co residing exactly in the middle of positions “a” and “b” shown in Fig. 4b of the main text.

S5. *Antisymmetric interlayer* exchange interaction in other materials systems

In addition to materials systems discussed in the main text, in order to examine the presence of the *antisymmetric* IEI in other material systems with different lateral ISB, here, we discuss two different materials systems of Pt/Co/Pt/Ir/Pt/Co/Pt and SAFs of Pt/CoSiB/Pt/CoSiB/Pt, with ferromagnetically and antiferromagnetically aligned layers due to the *symmetric* IEI. Similar measurements discussed in the main text were performed on the sample stacks. For these samples stacks, unlike the materials systems discussed in the main text, no height difference in the anomalous Hall effect (AHE) voltage is seen due to the identical thicknesses of the top and bottom ferromagnetic layers. Thus, the top and bottom magnetic layers are indistinguishable. Therefore, hereafter, we refer each magnetic layer to FM_1 and FM_2.

5.1. Pt/Co/Pt/Ir/Pt/Co/Pt grown by oblique sputtering

To explore the effect of the in-plane symmetry of multilayers on the ISB as well as the *antisymmetric* IEI, we prepare the multilayers of Ta(4)/Pt(4)/Co(1)/Pt(1.1)/Ir(t_{Ir})/Pt(1.1)/Co(1)/Pt(2)) (layer thicknesses in nanometers), where t_{Ir} = 0.3 and 0.75 nm for parallel and antiparallel couplings, respectively. For the purpose, particularly, we employ an oblique sputtering technique that allows us to control the direction of the sputtered atoms and possibly lower the in-plane symmetry. The most prominent effect of the technique is that it introduces tilted columnar structures, [9,10] as illustrated in Figure S8a. An interesting feature of the structure, we expect here, is that the columnar structure can have a broken inversion symmetry along the sputtering gradient axis. This may allow us to manipulate the IEI and the *antisymmetric* IEI in a controlled fashion. The oblique sputtering is performed with an oblique angle of α = 30° at which the target is tilted about 30° with respect to a substrate normal vector. We note that, here, the Ir layer is sputtered at the oblique angle without the rotation of sample holders during the growth, but for other layers, all are grown at

α = 0° (face-to-face configuration) with the sample rotation. Furthermore, as a reference sample, we also grow the samples where all layers are grown at the face-to-face configuration and with the sample rotation. The oblique sputtering is a well-established technique and its effect is studied in many systems.

Figure S8b-e shows the azimuthal-angular dependence of switching fields in SAFs with parallel and antiparallel coupling for both oblique sputtered and face-to-face sputtered thin films. The measurements are conducted with an in-plane field of $|\mu_0 H_{IN}|$ = 100 mT. For the oblique sputtered films, a unidirectional characteristic is observed for both SAFs with parallel and antiparallel coupling similar to that of the Pt/Co/Pt/Ru/Pt/Co/Pt in the main text. Most interestingly, we find that, for both SAFs with parallel and antiparallel couplings, the asymmetric axis **AS** of the samples all lies along the sputtering gradient direction where we expect the inversion symmetry is broken for the oblique sputtered samples. By contrast, we find that the direction of the **AS** is rather randomly distributed in the sample grown at the face-to-face configuration and exhibit much smaller amplitude.

By employing the oblique sputtering, we find that the orientation of the effective symmetry breaking and the *antisymmetric* IEI can be controlled. However, we expect a similar effect can be achieved by introducing, for example, a thickness gradient or an asymmetric grown by in-plane magnetic fields, which all lead to the effective symmetry breaking, and therefore, to the *antisymmetric* IEI, as demonstrated by our experiments and ab-initio calculations.

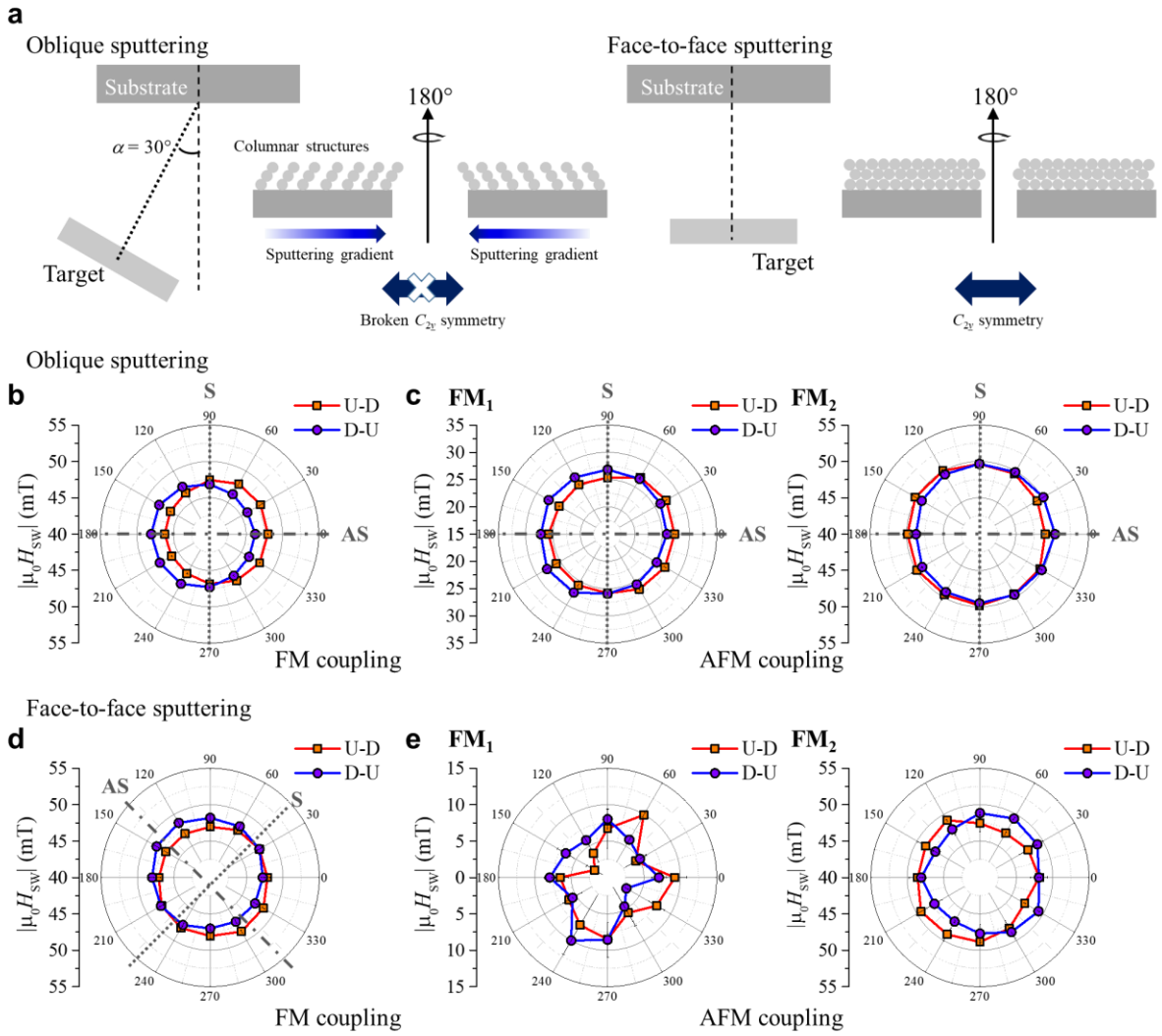

Figure S8 Chiral and unidirectional magnetization switching behaviors in synthetic antiferromagnet of Pt/Co/Ir/Co/Pt grown by oblique sputtering and face-to-face sputtering. a, Schematic illustrations of the oblique and face-to-face sputtering. For the oblique sputtering, Ir atoms are deposited at oblique angle of α = 30° which allows tilted columnar microstructure of thin films. The mirror symmetry of the tilted columnar microstructures is broken along the sputtering gradient axis. For the face-to-face sputtering, the targets are aligned normal to the surface of the substrate. **b-e,** Azimuthal-angular dependence of H_{SW} in synthetic antiferromagnets of Pt/Co/Pt/Ir/Co/Pt multilayers by the oblique (**b**) and (**c**) and face-to-face (**d**) and (**e**) sputtering with both parallel and antiparallel couplings. The H_{SW} is measured at a constant in-plane field of $|\mu_0 H_{IN}|$ = 100 mT. The oblique sputtered films had a tilt along the 0°-180° direction. **AS** and **S** represent asymmetric and symmetric axes, respectively.

5.2. Pt/CoSiB/Pt/CoSiB/Pt

In addition to materials systems discussed in the main text, in order to examine the presence of the *antisymmetric* IEI in other material systems, we used SAFs of Pt/CoSiB/Pt/CoSiB/Pt.[11] Similar measurements discussed in the main text were performed on the sample stacks of Ta(5)/Pt(3)/$Co_{75}Si_{15}B_{10}$(1.5)/Pt(t_{Pt})/$Co_{75}Si_{15}B_{10}$(1.5)/Pt(3), where t_{Pt} = 1.7 and 2.2 nm for which the *symmetric* IEI is ferromagnetic and antiferromagnetic, respectively.

Figure S9a and S9b show the azimuthal-angular dependence of switching fields in SAFs with parallel and antiparallel coupling, respectively. The measurements were conducted at the in-plane field of $|\mu_0 H_{IN}|$ = 50 mT and 100 mT, for SAFs with parallel and antiparallel coupling, respectively. Interestingly, an unidirectional behavior is clearly seen for both SAFs with parallel and antiparallel coupling as same as the SAFs of Pt/Co/Pt/Ru/Pt/Co/Pt stacks discussed in the main text, exhibiting an asymmetric **AS** along the direction of $\mathbf{H}_{IN}$ // 0° and 30° for SAF with parallel and antiparallel coupling, respectively. Particularly, for the antiparallel coupling case, the chiral nature of IEI in SAF of Pt/CoSiB/Pt/CoSiB/Pt multilayers is evidenced again from the remarkably distinct switching behavior – the opposite direction of the unidirectional switching – between FM_1 and FM_2, highlighting the presence of the *antisymmetric* IEI in SAFs of Pt/CoSiB/Pt/CoSiB/Pt multilayers.

The H_{IN} dependence of switching field H_{SW} is plotted in Fig. S9c and S9d. For both parallel and antiparallel coupling cases, an asymmetric behavior is seen when H_{IN} is applied along the **AS** axis, while a symmetric behavior is measured for $\mathbf{H}_{IN}$ // **S**. For the parallel coupling case, we found the difference in switching fields corresponding to $\Delta\mu_0 H_{sw} \approx 2.4$ mT between the positive and negative H_{IN} when $\mathbf{H}_{IN}$ // **AS**. For the antiparallel coupling, asymmetric curves with maxima (or minima) of H_{SW}, at $|\mu_0 H_{shift}| \approx 60$ mT were found in both

FM_1 and FM_2. We note that H_{shift} of FM_1 and FM_2 is found to be on the similar magnitude, in contrast to the results from Pt/Co/Pt/Ru/Pt/Co/Pt stack which shows a large difference in H_{shift} between the top and bottom layers (see Fig. 3b and 3d). This is due to the difference in material parameters between the top and bottom layers, e.g., the difference in perpendicular anisotropy arising from different interfacial qualities between top and bottom Co layers.

We would like to highlight that although the microscopic structure of Pt/CoSiB/Pt/CoSiB/Pt multilayers is different from the one of Pt/Co/Pt/Ru/Pt/Co/Pt, which may give rise to the difference in the magnitude of the *antisymmetric* IEI and its characteristic vector $\mathbf{D}_{inter}$, the *antisymmetric* IEI is commonly found in both sample structures. This evidences that the effective symmetry breaking is inevitable during the sample preparation of polycrystalline samples, therefore, giving rise to a finite amplitude of the effective *antisymmetric* IEI. Furthermore, we note that the crystalline structure of CoSiB on Pt is amorphous[12] while Co prefers (111) crystallographic texture[13]. Based on this fact, we speculate that the *antisymmetric* IEI is less sensitive to the microscopic structure of the ferromagnetic layers than the spacer non-magnetic layers with a relatively large spin-orbit coupling, as discussed in the main text.

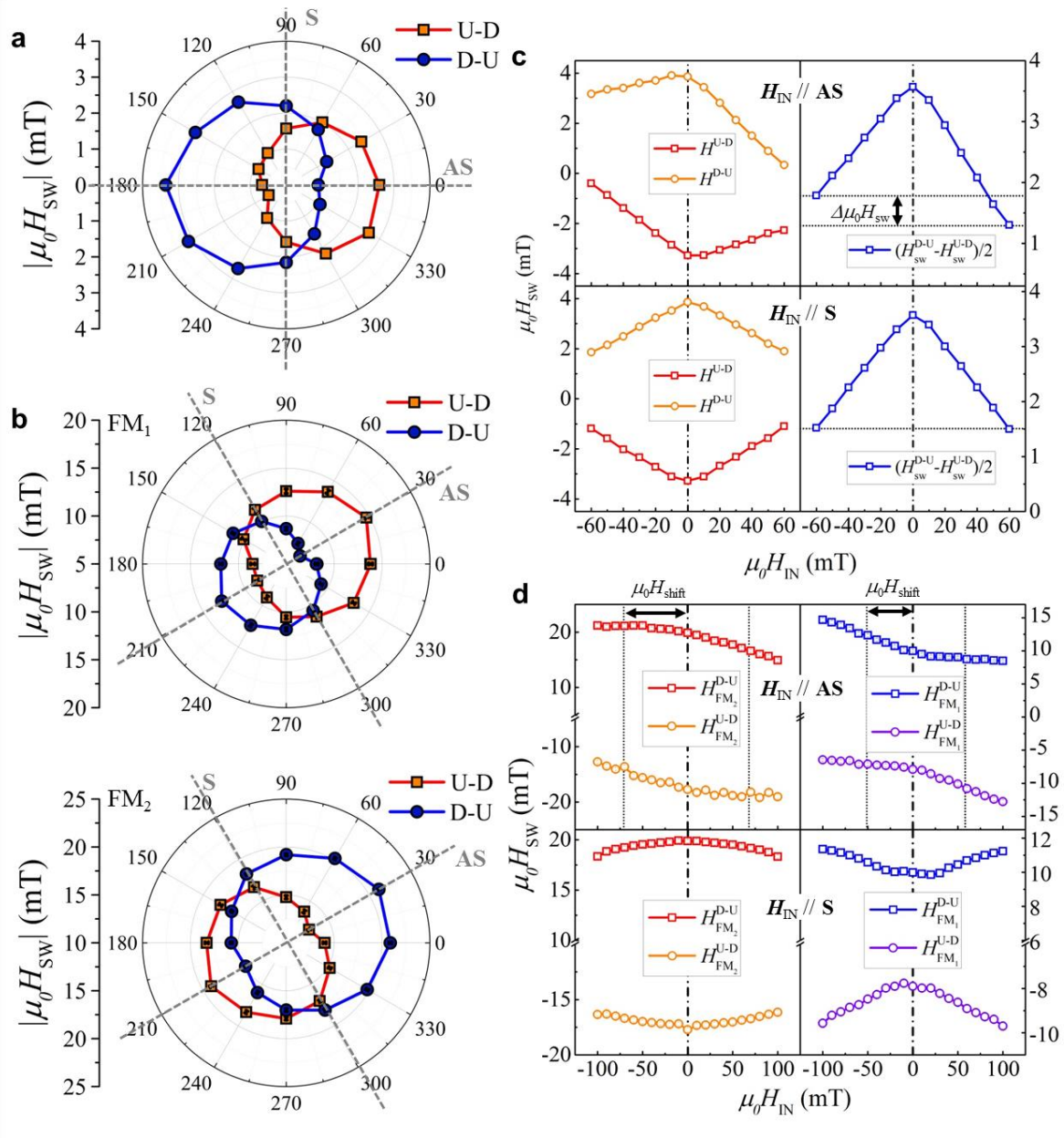

Figure S9 Chiral and unidirectional magnetization switching behaviors in synthetic antiferromagnets of Pt/CoSiB/Pt/CoSiB/Pt a, Azimuthal-angular dependence of switching field H_{SW} in synthetic antiferromagnet (SAF) of Pt/CoSiB/Pt/CoSiB/Pt with parallel coupling. The red and blue symbols represent the up-to-down (U-D) and down-to-up (D-U) switching fields respectively. The symmetric (**S**) and asymmetric (**AS**) axes correspond to the axis where the symmetric and unidirectional behaviors, respectively, are the most prominent. The H_{SW} is measured at a constant in-plane field of $|\mu_0 H_{IN}|$ = 50 mT and 100 mT, for SAFs with parallel and antiparallel coupling, respectively. **b**, Azimuthal-angular dependence of H_{SW} in SAFs with antiparallel coupling. The top and bottom panel correspond to ferromagnetic layer 1 (FM_1) and 2 (FM_2), respectively. **c**, The H_{SW} versus H_{IN}, applied along **AS** (top panel) and **S** (bottom panel) axes in SAFs with parallel coupling. The right panels on each column of (**c**) represent averaged $|H_{SW}|$ of U-D and D-U switching for H_{IN} and $-H_{IN}$, respectively. **d**, The H_{SW} versus H_{IN} in SAFs with antiparallel coupling. The H_{SW} for FM_2 and FM_1 are plotted on the left and

right panels of each column. For both parallel and antiparallel coupled cases, the symmetric (asymmetric) H_{SW} with respect to $H_{IN} = 0$ is found when H_{IN} is applied along **S** (**AS**) axis.

References:

1. Slonczewski, J. C. Fluctuation mechanism for biquadratic exchange coupling in magnetic multilayers. *Phys. Rev. Lett.* **67,** 3172–3175 (1991).

2. Marrows, C. H. & Hickey, B. J. Bilinear and biquadratic interlayer exchange coupling in sputtered Co/Cu multilayers damaged with residual gas impurities. *Phys. Rev. B* **59,** 463–467 (1999).

3. Emori, S., Bauer, U., Ahn, S.-M., Martinez, E. & Beach, G. S. D. Current-driven dynamics of chiral ferromagnetic domain walls. *Nat. Mater.* **12,** 611–616 (2013).

4. Je, S. G. *et al.* Asymmetric magnetic domain-wall motion by the Dzyaloshinskii-Moriya interaction. *Phys. Rev. B* **88,** 214401 (2013).

5. Han, D. S. *et al.* Asymmetric hysteresis for probing Dzyaloshinskii-Moriya interaction. *Nano Lett.* **16,** 4438–4446 (2016).

6. Lo Conte, R. *et al.* Role of B diffusion in the interfacial Dzyaloshinskii-Moriya interaction in Ta/Co20Fe60B20/MgO nanowires. *Phys. Rev. B* **91,** 14433 (2015).

7. Landau L. D., Lifshitz E. M., P. L. P. *Electrodynamics of Continuous Media*. (Elsevier, 2004).

8. Schweflinghaus, B., Zimmermann, B., Heide, M., Bihlmayer, G. & Blügel, S. Role of Dzyaloshinskii-Moriya interaction for magnetism in transition-metal chains at Pt step edges. *Phys. Rev. B* **94,** 24403 (2016).

9. Barranco, A., Borras, A., Gonzalez-Elipe, A. R. & Palmero, A. Perspectives on oblique angle deposition of thin films: From fundamentals to devices. *Prog. Mater. Sci.* **76,** 59–153 (2016).

10. Alvarez, R. *et al.* Nanostructured Ti thin films by magnetron sputtering at oblique angles. *J. Phys. D. Appl. Phys.* **49,** 045303 (2016).

11. Choi, Y. *et al.* Oscillatory Interlayer Exchange Coupling in Amorphous CoSiB/Pt/CoSiB Structure. *IEEE Trans. Magn.* **51,** 1–4 (2015).

12. Kim, T. W. *et al.* Perpendicular magnetic anisotropy of amorphous [CoSiB/Pt]N thin films. *J. Appl. Phys.* **117,** 17B502 (2015).

13. Emori, S. & Beach, G. S. D. Optimization of out-of-plane magnetized Co/Pt multilayers with resistive buffer layers. *J. Appl. Phys.* **110,** 33919 (2011).